

Earth and Planetary Science Letters 194 (2002) 311-326

**EPSL** 

www.elsevier.com/locate/epsl

# A 13 200 year history of century to millennial-scale paleoenvironmental change magnetically recorded in the Palmer Deep, western Antarctic Peninsula

Stefanie A. Brachfeld a,\*, Subir K. Banerjee b, Yohan Guyodo c, Gary D. Acton d

<sup>a</sup> Byrd Polar Research Center, Ohio State University, 108 Scott Hall, 1090 Carmack Road, Columbus, OH 43210, USA
<sup>b</sup> Institute for Rock Magnetism, Wincell School of Earth Sciences, University of Minnesota, Minneapolis, MN, USA
<sup>c</sup> Department of Geological Sciences, University of Florida, Gainesville, FL, USA
<sup>d</sup> Ocean Drilling Program, Texas A&M University, College Station, TX, USA

Received 6 July 2001; received in revised form 23 October 2001; accepted 23 October 2001

#### **Abstract**

A 13 200-yr record of magnetic parameters from the Palmer Deep, western Antarctic Peninsula, records a sequence of five distinct shifts in glacimarine sedimentation coupled with century-scale variations in paleoproductivity. The five major shifts are manifested as abrupt, order of magnitude changes in low-field magnetic susceptibility, accompanied by changes in magnetic particle size and mineralogy. The Late Holocene (3.4-0 ka), the Early Holocene (11.5-9 ka), and the Last Glacial Maximum (prior to 13.2 ka) are intervals of strong low-field magnetic susceptibility and are characterized by multi-domain (MD) magnetite. MD magnetite is associated with zones of abundant gravel grains and is interpreted here as an indicator of material transported as ice-rafted debris. Deglaciation (13.2–11.5 ka) and the Middle Holocene (9–3.4 ka) were times of enhanced productivity. The Middle Holocene marks the onset of centuryscale productivity cycles seen in high-field magnetic susceptibility, which is responding to variations in biogenic silica. Deglaciation and the Middle Holocene interval contain pseudo-single domain magnetite and titanomagnetite, respectively. These observations are surprising given the abundance of coarse MD magnetite available in local source rocks. The magnetic mineral assemblage in the Deglaciation interval, however, can be explained by density sorting in meltwater plumes. During the Middle Holocene, the magnetic mineral assemblage suggests the reduction or cessation of locally derived terrigenous sediment, and by inference, the reduction or cessation of iceberg generation. The Early Holocene-Middle Holocene shift in terrigenous sedimentation may be responding in part to sea level, which controls the position of the grounding line. The Palmer Deep Late Holocene interval coincides with the Neoglacial period, a time of glacier re-advances worldwide. © 2002 Elsevier Science B.V. All rights reserved.

Keywords: magnetic susceptibility; magnetic domains; Antarctic Peninsula; Holocene; paleoclimatology; Leg 178

1. Introduction

\* Corresponding author. Tel.: +1-614-247-6843; Fax: +1-614-292-4697.

E-mail address: brachfeld.2@osu.edu (S.A. Brachfeld).

The Southern Ocean and the Antarctic cryosphere occupy central roles in global oceanic

0012-821X/02/\$ – see front matter  $\ @$  2002 Elsevier Science B.V. All rights reserved.

PII: S0012-821X(01)00567-2

and atmospheric dynamics. The Southern Ocean is the world's most productive ocean. The Antarctic margin is a source of deep water that drives ocean circulation. Antarctica is one of the windiest, stormiest places on Earth. These systems affect the mixing of surface waters and mediate the break up and dispersal of sea ice. The East Antarctic Ice Sheet (AIS) and West AIS contain a 60-m and 6-m (respectively) equivalent in global sea level rise [1]. Historic and recent trends observed in Antarctica highlight the need to understand the natural cycles of environmental variability and the response of the AIS to global climate change.

The Antarctic Peninsula region has experienced particularly rapid environmental changes over the past half century. This region has experienced a warming trend, decreases in ice-shelf extent and stability, and changes in sea-bird distribution ([2] and references therein). The cause of these changes is presently unknown, but may involve both natural and anthropogenic components. Therefore, it is necessary to obtain past records of environmental conditions in order to understand the natural degree of variability at decadal and century time scales.

Shelf basins and fjords on the western margin of the Antarctic Peninsula have proven to be repositories of thick Holocene sediment sequences (e.g. [3-5]). The Palmer Deep, an inner shelf basin, is particularly well situated to monitor paleoenvironmental conditions. The Palmer Deep is a sediment trap that preserves records of biological productivity and glacial sedimentation. The Palmer Deep is located near the Antarctic circum-polar current and the Antarctic convergence. The Palmer Deep is exposed to storm systems that move through the Amundsen and Bellingshausen Seas. The sedimentary sequence recovered from the Palmer Deep during Ocean Drilling Program (ODP) Leg 178 represents the first glacimarine record of comparable resolution to ice core records, and is the first such record from high southern latitudes.

Here we focus on the distinctive magnetic susceptibility profile from the Palmer Deep, which appears to be characteristic of glacimarine sediments from the western Antarctic Peninsula [3]. In the Palmer Deep (ODP Site 1098) we have

the opportunity to integrate a Holocene to Late Pleistocene record of rock magnetic parameters with a wide array of floristic, sedimentologic, and geochemical proxies such as diatom assemblages, benthic foraminifera assemblages, biogenic silica abundance, stable isotopes of oxygen, carbon, and nitrogen, elemental abundance, and particle size [6-17]. This aids in the development of linkages between magnetic parameters and environmental conditions. Whereas most of the proxies listed above track biogenic sedimentation and hydrography, magnetic parameters contain information regarding the abundance, grain size, and mineralogy of the terrigenous material supplied to the Palmer Deep, and by inference, information regarding sediment transport mechanisms. This study presents a continuous 13 200-yr time series of magnetic parameters that record five distinct paleoclimate intervals, on which are superimposed century-scale cycles in biogenic sedimentation. We evaluate the roles of paleoproductivity, ice rafting, sediment provenance, and post-depositional diagenesis in controlling features of this regional susceptibility signal.

# 2. Site description and stratigraphy

The Palmer Deep is a bathymetric depression located 20 km southwest of Anvers Island (Fig. 1). It consists of two fault-bounded 1000–1400-m-deep basins (Basin I and Basin II/III), separated by a 750-m-deep sill [18,19]. High-resolution acoustic surveys indicate a draped sediment fill in Basin I and a ponded geometry in Basin II/III [18,19]. ODP Leg 178 collected three hydraulic piston cores from Site 1098 in the southern end of Basin I (64°51.7235′S, 64°12.4712′W, 1012 m at Site 1098 Hole A) [19], the shallowest and narrowest of the sub-basins.

The composite Holocene sediment section at Site 1098 consists of 47 m of olive green to dark olive green diatomaceous mud/ooze overlying a diamicton [19]. The upper 25 meters composite depth (mcd) alternates between structureless and laminated intervals (Fig. 2). Three turbidites interrupt the section below 24.90 mcd, hereafter denoted T1 (24.91–28.89 mcd), T2 (31.98–33.22)

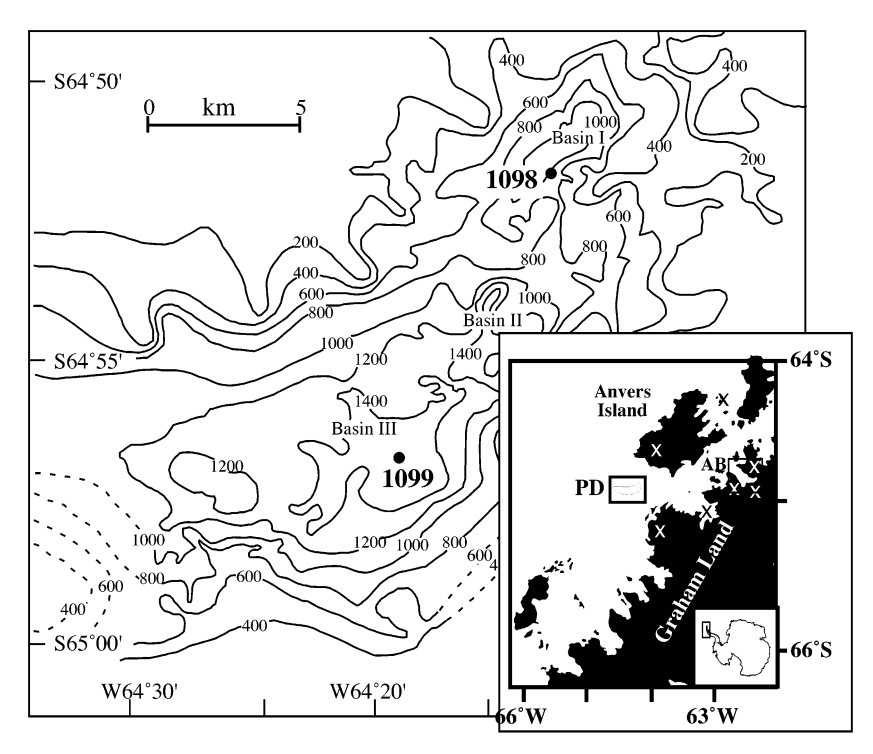


Fig. 1. Location of the Palmer Deep (PD), Andvord Bay (AB) and rock sample sites (denoted X) on the western Antarctic Peninsula.

mcd), and T3 (40.74–40.99 mcd), with thickness varying slightly in each of the three Holes [19]. The interval 33.22–41 mcd is largely structureless and displays high gravel grain counts. Below T3, the interval 41.00–47.3 appears to be rhythmically laminated [14,15]. The base of the core below 47.3 mcd consists of a massive diamicton (Fig. 2) [19].

#### 3. Chronology

Radiocarbon dating of acid-insoluble sedimentary organic carbon and foraminiferal calcite from several cores collected by the United States Antarctic Program and during ODP Leg 178 contributed to the Palmer Deep chronology. A discussion of the dated material, derivation of a reservoir correction (1230 yr), and the conversion to calendar ages is presented in [6]. The depth–age model presented here (Fig. 2) was constructed from [6] (table 1).

The mcd scale was constructed by correlating magnetic susceptibility, bulk density, and color variations between the three cores collected at Site 1098 [20]. The progression of ages in the upper 25 mcd suggests continuous sedimentation over the past 9000 yr. The age model below 25 mcd is less certain due to the presence of three turbidites. Turbidite 1 consists of ~4 mcd of massive diatomaceous mud with no evidence of erosion at its base. Therefore, we have removed T1 and concatenated the remaining section. The depth-age data from 0 mcd to the top of T2 were fit with a third order polynomial (Fig. 2). Turbidite 2 has a sand and gravel layer at its base. This turbidite likely eroded some underlying material [19]. We used a linear regression between T2 and T3 (Fig. 2) and extrapolated this trend up to the base of T2. The resulting age model suggests 500 yr of missing section below T2.

The interval from the bottom of T3 to the base of the core was difficult to model. The depth–age

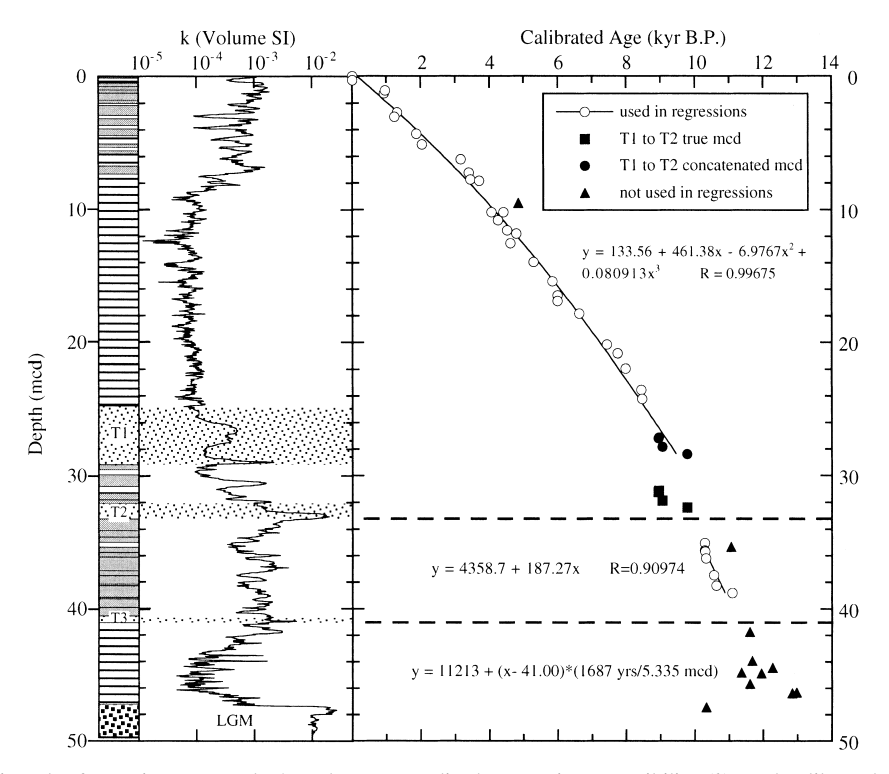


Fig. 2. Core stratigraphy from Site 1098 Hole A, volume-normalized magnetic susceptibility (k), and calibrated radiocarbon dates [6] from the Palmer Deep. Solid gray intervals denote massive, structureless intervals. Horizontal lines denote laminated intervals. A third order polynomial and a linear regression were fit to the depth-age data from [6] in order to construct a chronology from 0 to 32 mcd and 33 to 40.0 mcd, respectively. Solid triangles denote data points that were not used in the regressions. Below T3 we applied a constant sedimentation rate of 0.316 cm/yr determined from the ages at the top and bottom of the laminated interval.

data show numerous age reversals (older over younger) (Fig. 2). T3 is thin and does not appear to have an erosional base [19]. We assumed zero erosion and assigned the sediment immediately below T3 the same age as the sediment immediately above T3 (11213 yr BP). We calculated a sedimentation rate using the age of 11213 yr BP at the base of T3 and an age of 12900 yr BP at the base of the diatomaceous ooze (the average of two closely spaced radiocarbon dates immediately above the diamict).

#### 4. Methods

Whole-core physical properties measurements, consisting of low-field volume-normalized magnetic susceptibility (k), bulk density (GRAPE),

natural gamma radiation (NGR), and p-wave velocity, were made onboard the R.V. JOIDES Resolution during ODP Leg 178 using an automated Multisensor Track [19]. Subsamples were collected every 10 cm from Site 1098 Hole A and freeze-dried for magnetic granulometry analyses performed at the Institute for Rock Magnetism at the University of Minnesota. Low-field massnormalized susceptibility  $(\chi_{LF})$  was measured using a Geofyzika KLY-2 Kappabridge. Hysteresis parameters, high-field mass-normalized susceptibility  $(\chi_{HF})$ , and Curie temperatures were measured on a Princeton Measurements Corp. Micro Vibrating Sample Magnetometer. Curie temperatures were determined from the temperature dependence (0-700°C) of the saturation magnetization  $(M_S)$  of a sample in a 1-T field. Measurements were made in a helium gas atmosphere.

Low-temperature (20–300 K) remanence and susceptibility measurements were made using a Quantum Design MPMS-XL Susceptometer.

#### 5. Controls on magnetic susceptibility

The low-field volume-normalized magnetic susceptibility (k) profile of Site 1098 displays five distinct zones in which k alternates between strong and weak values, paralleled by abrupt shifts in magnetic domain state (Fig. 3). Using these two proxies, the zones are defined here as the Last Glacial Maximum (LGM) represented by the diamict deposited prior to  $\sim 13.2$  ka, the Deglaciation interval (13.2–11.5 ka), the Early Holocene interval (11.5–9 ka), the Middle Holocene interval (3.4 ka to present). The motivation for this rock magnetic study is to investigate the controls on the magnetic susceptibility record from Site 1098 in order to interpret its environmental signal.

# 5.1. Abundance of ferromagnetic, paramagnetic, and diamagnetic components

In a three-component assemblage of ferromagnetic minerals (F – iron oxides), paramagnetic minerals (P – clay minerals and 'non-magnetic' iron-bearing minerals), and diamagnetic minerals (D – quartz, calcite, biogenic silica, water), the bulk low-field mass-normalized susceptibility can be represented as:

$$\chi = N_{\rm D}\chi_{\rm D} + N_{\rm P}\chi_{\rm P} + N_{\rm F}\chi_{\rm F} \tag{1}$$

where  $N_i$  and  $\chi_i$  are the mass fraction and average susceptibility of each component. Ferromagnetic susceptibility ( $\chi_F$ ) is a complex function of several variables including the concentration of ferromagnetic material, ferromagnetic particle size, mineralogy, and the measurement conditions (temperature, applied field properties). Ferromagnetic minerals account for less than 1% by mass of typical sediment assemblages. However,  $\chi_F$  is several orders of magnitude stronger than paramag-

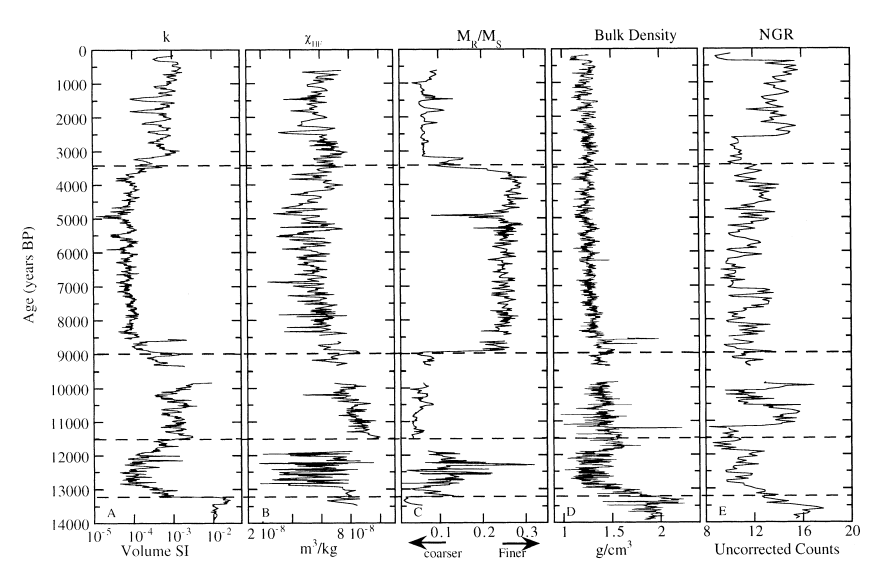


Fig. 3. Whole-core volume-normalized magnetic susceptibility (k), mass-normalized high-field susceptibility  $(\chi_{\rm HF})$ , the hysteresis parameter saturation remanence normalized by saturation magnetization  $(M_{\rm R}/M_{\rm S})$ , bulk density (GRAPE), and natural gamma radiation (NGR) profiles for Site 1098. The gap at 9300–9800 yr BP is due to erosion at the base of turbidite 2 (T2). The positive correlation between k and GRAPE values (R=0.775) suggests that fluctuations in the low-density, diamagnetic, biogenic silica content are an important control on the short-wavelength (century and decadal scale) features in the Site 1098 susceptibility profile. However,  $\chi_{\rm HF}$  shows no significant changes at the zone boundaries seen in the k record, suggesting that dilution with biogenic silica is not the sole control on k. In contrast, significant changes occur in  $M_{\rm R}/M_{\rm S}$  at zone boundaries. This parameter shows a small fluctuation prior to the stabilization of Late Holocene conditions and a coarse-grain 'excursion' at 4.9–5 ka.

netic and diamagnetic susceptibility ( $\chi_P$  and  $\chi_D$ ). The term  $N_F\chi_F$  generally controls the susceptibility signal (k) measured in typical pass-through sensors (room temperature, weak 50- $\mu$ T applied field). When k is dominated by  $\chi_F$ , the use of k to monitor a diamagnetic component of the sediment assemblage, such as biogenic silica, can be complicated by coeval variations in the other variables.

Paramagnetic and diamagnetic components of a sediment assemblage can be examined directly by measuring high-field magnetic susceptibility ( $\chi_{HF}$ ). When the applied field (H=1 T for this study) exceeds the saturating field of ferromagnetic minerals, then  $\chi_F$  is zero and  $\chi_{HF}$  is given by:

$$\chi_{\rm HF} = N_{\rm P} \chi_{\rm P} + N_{\rm D} \chi_{\rm D} \tag{2}$$

Therefore,  $\chi_{HF}$  is more responsive to variations in biogenic silica and hence productivity variations, provided that there are minimal fluctuations in the detrital diamagnetic:paramagnetic ratio.

A comparison of k with  $\chi_{HF}$  indicates that variable dilution of terrigenous material with biogenic silica cannot account entirely for the abrupt, large variations in k that define the five zones (Fig. 3). The average value of k during the Middle Holocene is a factor of 10–20 less than the average value of k during the Late Holocene and the Early Holocene, and a factor of  $\sim 50$  less than the k peaks in those two intervals. If a factor of 50 reduction in  $N_{\rm F}$  occurred in direct response to a factor of 50 increase in biogenic silica  $(N_D)$ , for which  $\chi_D$  is negative, then it should cause a noticeable decrease in  $\chi_{HF}$ . While  $\chi_{HF}$  does show high-frequency oscillations with wavelengths of 200-400 yr, there are no abrupt, large changes at zone boundaries.

The expected variations in  $\chi_{HF}$  could be masked if the paramagnetic component, for which  $\chi_P$  is positive, was increasing along with the diamagnetic component. To evaluate this hypothesis we examined a down-core profile of NGR measured onboard the *Resolution*. NGR detects gamma radiation emitted during the decay of radioactive isotopes such as  $^{40}$ K and radioactive elements in the uranium and thorium decay series. These ions are large and incompatible in most

crystal structures, but can be accommodated within or adsorbed onto clay minerals. Therefore, increases in gamma radiation are ascribed to clay minerals.

An increase in the proportion of clay minerals during the Middle Holocene would be required to counteract the expected decreases in  $\chi_{HF}$  and bulk density due to increases in biogenic silica. The Palmer Deep NGR profiles indicate a decrease in the proportion of clay minerals during the Middle Holocene and during the Deglaciation interval (Fig. 3E). Therefore, the increase in diamagnetic biogenic silica is not offset by a parallel increase in the paramagnetic component. Rather, a reduction in the paramagnetic component contributes to the low values of whole-core susceptibility.

Alternatively, the abundance of ferromagnetic minerals could be decreased by dissolution due to iron–sulfur diagenesis. During iron–sulfur diagenesis the ferric iron in magnetite is reduced to ferrous iron in solution, which later precipitates as a less magnetic or non-magnetic Fe<sup>2+</sup>-carrying mineral such as ferrimagnetic greigite, pyrrhotite, or paramagnetic pyrite [22]. In this scenario the susceptibility would be reduced without requiring enormous changes in the terrigenous/biogenic ratio. However, interstitial water profiles (Fig. 4) collected onboard the *Resolution* during ODP Leg 178 indicate that organic matter degradation and sulfate reduction begin at 20–30 mcd [19],

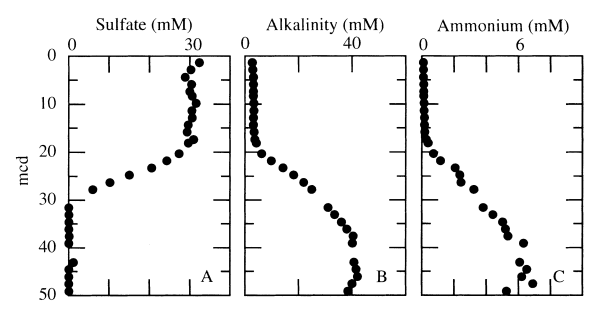


Fig. 4. Interstitial water chemistry from Site 1098, Hole C. (A) Alkalinity and (B) ammonium byproducts of organic matter degradation, increase at  $\sim 20$  mcd. (C) Sulfate concentrations indicate the onset of sulfate reduction at  $\sim 18$  mcd. Iron was consistently below the detection limit of the instrument on the *Resolution*. No chemical boundaries coincide with the boundaries of susceptibility zones.

substantially deeper than the Middle Holocene—Late Holocene transition. We did not detect magnetic iron sulfides, the intermediate products of iron–sulfur diagenesis (see Section 5.3).

Coarse multi-domain (MD) magnetite is abundant in the sediment overlying and underlying the Middle Holocene interval (see Section 5.2). We find it unlikely that coarse > 10-micron grains would completely dissolve in only a few thousands years. Furthermore, fine-grained pure magnetite is abundant in the Deglaciation interval at the base of Site 1098 (see Section 5.3). If we were to accept the dissolution hypothesis for coarse MD magnetite in the Middle Holocene interval, then the fine-grained magnetite at the base of the core certainly would not have survived. Therefore, we find that dissolution of magnetite is not a major control on the rock magnetic record. The explanation may lie in particle size and/or mineralogy variations, which we discuss below.

## 5.2. Magnetic 'grain size'

Magnetic hysteresis parameters indicate that there are shifts in magnetic domain state, which is a function of grain volume, between each of the five susceptibility zones (Fig. 3C). These shifts are most clearly seen in the ratio of saturation remanence  $(M_R)$  normalized by saturation magnetization  $(M_S)$ . During the Late Holocene interval,  $M_{\rm R}/M_{\rm S}$  values fluctuate between 0.05 and 0.10, which straddles the boundary between MD and pseudo-single domain (PSD) behavior assuming a magnetite carrier [23]. Hysteresis parameters from the Middle Holocene interval have much higher values of  $M_R/M_S$  (0.20–0.30) than the overlying and underlying intervals, suggesting either a change in provenance from a coarsegrained to a fine-grained source rock, a change in mineralogy to a mineral with higher magnetocrystalline anisotropy, or a change in the mechanism of sediment transport to the Palmer Deep. We observed one brief coarse-grained 'excursion' at 4.9-5.0 ka (Fig. 3C). This coincides with diatom evidence of a cool phase within the Middle Holocene from 5.5 to 4.7 ka [11,12]. However, the magnetic expression of this feature is restricted to only three samples.

Hysteresis parameters from the turbidites, from the Early Holocene interval, and the diamicton (below 47.3 mcd) are clearly MD, with  $M_{\rm R}/M_{\rm S}$  values of 0.03–0.05. The Deglaciation interval is generally PSD with slightly higher values of  $M_{\rm R}/M_{\rm S}$  than low-k Late Holocene intervals, although MD values are also observed. On average, the Deglaciation interval contains finer material than the underlying diamicton and overlying cooling reversal.

## 5.3. Magnetic mineralogy

Many magnetic minerals undergo magnetic order/disorder transitions and crystallographic phase transitions (such as at Curie temperatures, Néel temperatures, magnetic isotropic points, the Verwey transition and the Morin transition) at temperatures ranging from 10 to 1000 K, that can be used as diagnostic indicators of a mineral's presence or absence (see [24] for full discussion). Low-temperature analyses consisted of a pair of measurements. First, a sample was cooled in zero applied field from 300 to 20 K, given a 2.5-T saturation remanence at 20 K, and  $M_R$  was then measured during warming to 300 K. The sample was then cooled back down to 20 K, this time in the presence of a 2.5-T applied field, and  $M_R$  was re-measured during warming to 300 K. This zerofield-cooled (ZFC) and field-cooled (FC) pair of measurements, described in detail in [25], have proven useful in evaluating magnetic domain state and particle size, and detecting the presence of intact chains of stable single domain (bacterial) magnetite.

Samples from the Late Holocene, the Early Holocene, the LGM, and the turbidites, all intervals of high k values, display sharp magnetite Verwey transitions at 108–118 K (Fig. 5A).  $M_{\rm R}$  decreases by 40–70% across the Verwey transition. In addition, the FC curves are consistently lower than the ZFC curves. This is unexpected, since cooling in the presence of an applied magnetic field should provide a bias to only one of the six [100] easy axes of magnetization upon cooling through the Verwey transition and increase the efficiency of remanence acquisition. However, we have observed this behavior in several natural and

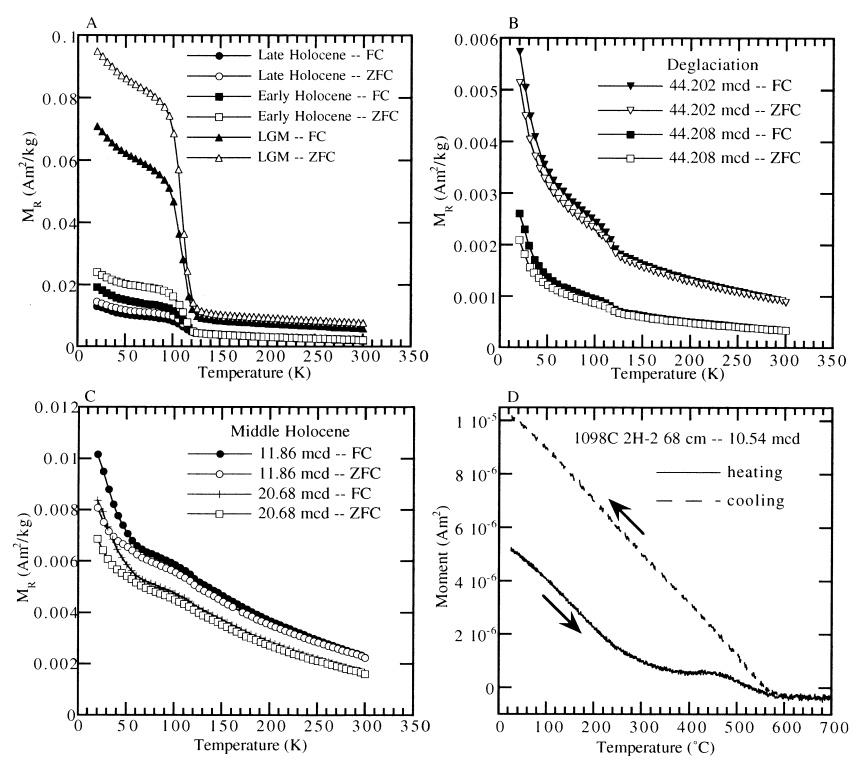


Fig. 5. Low-temperature (K) remanence measurements from (A) the Late Holocene (2.02 mcd), Early Holocene (34.32 mcd), and LGM (48.04 mcd), (B) Deglaciation, and (C) the Middle Holocene, and (D) high-temperature (°C) thermomagnetic curves from the Middle Holocene. All susceptibility zones except the Middle Holocene display the magnetite Verwey transition at 108-118 K. The Middle Holocene shows no diagnostic low-temperature transitions. High-temperature thermomagnetic curves from the Middle Holocene display  $M_{\rm S}$  drops at  $290-300^{\circ}{\rm C}$  and  $\sim 450-580^{\circ}{\rm C}$ , suggesting titanium-rich titanomagnetite.

synthetic samples, and it appears to be a characteristic of MD magnetite.

The Deglaciation interval is also characterized by magnetite (Fig. 5B). The shape of the  $M_R$ -T curves is much different than those of the other intervals. The Deglaciation samples show a rapid loss of remanence between 20 and 50 K, which could indicate superparamagnetic (SP) particles. The Verwey transition is broader than in the intervals discussed above.  $M_R$  decreases by 10–15% across the Verwey transition and the FC curve is slightly higher than the ZFC curve. All of these observations are consistent with an assemblage of fine PSD particles, possibly in combination with SP particles.

The Middle Holocene interval contains a very different magnetic mineralogy. Brachfeld and Banerjee [21] reported the presence of titanium-rich titanomagnetite and the complete absence

of magnetite at the tail end of the Middle Holocene interval, immediately below the abrupt shift in k at 3400 yr BP. Here we find that this assemblage persists for the entire Middle Holocene interval. The Middle Holocene samples have no clear diagnostic low-temperature behavior but resemble the low-temperature  $M_R$ -T curves of synthetic TM60 (Fe<sub>3-0.6</sub>Ti<sub>0.6</sub>O<sub>4</sub>, where x = 0.6 is the ulvöspinel content) [26]. The presence of titaniumrich titanomagnetite is confirmed by high-temperature measurements. High-temperature thermomagnetic curves show a significant decay in the saturation magnetization from room temperature to  $\sim 300$ °C, then a second interval of decay from ~440 to 580°C (Fig. 5D). The loss of magnetization at 290-300°C corresponds to the Curie temperature of approximately TM41. However, TM41 does have a diagnostic low-temperature isotropic point at  $\sim 70$  K [26], whereas we observed no noteworthy features from 20 to 300 K (Fig. 4C). One possible explanation is that there is some degree of oxidation of the titanomagnetite. Oxidation of magnetite broadens and suppresses the Verwey transition and may affect the isotropic point as well [27]. Oxidation also raises the Curie temperature of titanomagnetites [28]. An apparent Curie temperature of 300°C could indicate TM60 with an oxidation parameter of ~0.5.

The susceptibility of compositions TM40 to TM60 is a factor of  $\sim 1.6$ –30 less than that of pure magnetite [29,30], which is largely responsible for the very low values of k in the Middle Holocene interval. An unresolved question is whether titanomagnetite is present in the other susceptibility zones. Titanium-rich titanomagnetite is present in mafic dikes, volcanics, and in oceanic crust along the Antarctic Peninsula, although it has yet to be determined which source rocks match the phase in the Palmer Deep ([31], S. Brachfeld, unpublished data). Given its weaker magnetization and susceptibility, titanomagnetite may be present, but masked in the high-susceptibility zones.

#### 6. Discussion

Each of the five susceptibility zones is characterized by a distinct magnetic mineral assemblage. Magnetic granulometry primarily reflects terrigenous sediment sources and transport mechanisms. Comparison of the magnetic data with micropaleontological and geochemical data enables the development of a broader picture of environmental conditions.

#### 6.1. LGM (> 13.2 ka)

The massive diamicton at the base of Site 1098 contains 1–1.5% magnetite, a concentration equivalent to the abundance in local source rocks [31]. Hysteresis parameters and low-temperature measurements indicate very coarse MD magnetite. Rock magnetic parameters cannot distinguish emplacement mechanisms, for example whether this unit represents a basal till or a proximal glacimarine unit deposited beneath a floating ice shelf.

However, the magnetic abundance and particle size observations suggest very little or no density sorting of this unit, consistent with an environment very close to the grounding line. For this reason, we interpret the diamict as representing the LGM even though the age of the deposit is more consistent with the Antarctic Cooling Reversal (ACR) recorded in ice cores [32]. Depositing this diamict during the short ACR would be difficult in the Palmer Deep, requiring a very rapid response of the ice sheet to atmospheric conditions and a very large increase in ice volume in order to ground at Site 1098. Furthermore, the diamict-ooze transition age of 13 200 yr BP is consistent with other estimates of ice retreat from the western margin of the Antarctic Peninsula [33].

#### 6.2. Deglaciation (13.2–11.5 ka)

The Deglaciation interval marks the onset of marine deposition following the retreat of grounded ice. This interval is strongly laminated throughout due to alternations between terrigenous-rich and pure diatomaceous ooze laminae [11–15]. The laminae display large fluctuations in  $\chi_{\rm HF}$  of identical trend and amplitude to the variations in bulk susceptibility (Fig. 3). The magnetic particle size is PSD–MD in both terrigenous layers and biogenic layers. In this interval the diamagnetic phases exert the main control on k.

Diatomaceous laminae indicate a move towards open marine conditions and an environment seaward of the glacial calving front. At this time the Palmer Deep may have been a more ice-proximal environment than at present, receiving terrigenous material from debris-laden meltwater that deposited better sorted and finer magnetic grains relative to the coarser grains in the overlying and underlying zones. The influx of fresh meltwater likely contributed to stratification of the water column, creating conditions conducive to diatom blooms.

#### 6.3. Early Holocene (11.5–9 ka)

The Early Holocene interval is characterized by a return to high values of k and the deposition of

coarser MD grains, although the concentration of magnetic material is lower than the LGM and the particle size is finer than the LGM. Gravel grain counts, interpreted as ice-rafted debris (IRD), are high [6]. MD magnetite consistently occurs in tandem with high gravel grain counts throughout the entire sedimentary sequence. Therefore, we suspect that coarse, dense, MD magnetite is carried to the Palmer Deep as IRD. This zone marks the onset of turbidite deposition at Site 1098 [19]. This could be indicative of re-advancing glaciers that triggered mass flows across the shelf and down the steep sides of the Palmer Deep. However, these turbidites could also be a result of movement along the basin's bounding normal faults [18]. Diatom abundance and % opaline silica are lower than in the underlying and overlying intervals [9-13], indicating decreased productivity with respect to the Deglaciation and Middle Holocene. However, diatom abundance and inferred levels of productivity are higher than present levels [11].

#### 6.4. Middle Holocene (9-3.4 ka)

The Middle Holocene interval contains PSD titanium-rich titanomagnetite that may be partially oxidized. Pure magnetite is absent. This shift in magnetic mineralogy indicates a change in terrigenous provenance, which is supported by changes in elemental ratios of Fe, Ti, and Al [16]. Gravel counts are low [6]. Diatom abundance and opal mass accumulation rates are very high during the Middle Holocene [9-13]. Furthermore, diatom assemblages contain species that indicate the southward incursion of warmer northern surface waters into the Palmer Deep [13]. Calcareous foraminifera are absent [7,8]. Shevenell and Kennett [7] suggest that the absence of calcareous foraminifera correlates with the presence of corrosive Upper Circum-polar Deep Water, an old, warm water mass that is corrosive to calcite but nutrient-rich and conducive to phytoplankton blooms. The Middle Holocene was clearly a time of enhanced productivity and reduced terrigenous sedimentation in the Palmer Deep.

Superimposed on the overall elevated produc-

tivity levels are century-scale cycles that begin in the Early-Middle Holocene and continue through the present. Visual inspection of  $\chi_{\rm HF}$  during the Middle Holocene shows the presence of features with 200-400-yr wavelengths (Fig. 3).  $\chi_{\rm HF}$  reflects the biogenic silica content of the sediment and is unaffected by the complicating particle size and mineralogy influences that mute the k signal during the Middle Holocene. Therefore,  $\chi_{\rm HF}$  is the more appropriate magnetic parameter for tracking paleoproductivity cycles.

The periodic lows in  $\chi_{\rm HF}$  correlate with diatomaceous laminae [11–13]. Diatom blooms are typically associated with enhanced water column stability, which may be due to several underlying causes. The water column may be thermally stratified in response to atmospheric warming, or stratified due to the presence of low-density meltwater from sea ice or glacial ice. In addition, the mixing depth may have been greatly reduced during the Middle Holocene if the frequency and intensity of storms were less than today [3].

#### 6.5. Late Holocene (3.4 ka to present)

The magnetic properties of the Late Holocene interval have been discussed in detail previously [3,21]. Briefly, high values of k are a function of increased terrigenous sedimentation. Variable dilution of terrigenous material with biogenic silica causes the regularly spaced large-amplitude variations in k, which are the continuation of  $\chi_{\rm HF}$  cycles initiated in the Middle Holocene. The interval is marked by the reappearance of MD magnetite and elevated gravel grain counts.

#### 6.6. Global implication of the Palmer Deep record

The 13 200-yr succession recovered from the Palmer Deep records a sequence of five major shifts in sedimentation. The sequence consists of three intervals dominated by terrigenous glacial sedimentation (LGM, Early Holocene, Late Holocene), and two intervals dominated by biogenic sedimentation (Deglaciation, Middle Holocene). The Late Holocene interval in the Palmer Deep coincides with the Neoglacial period, the widely documented re-advance of mountain glaciers

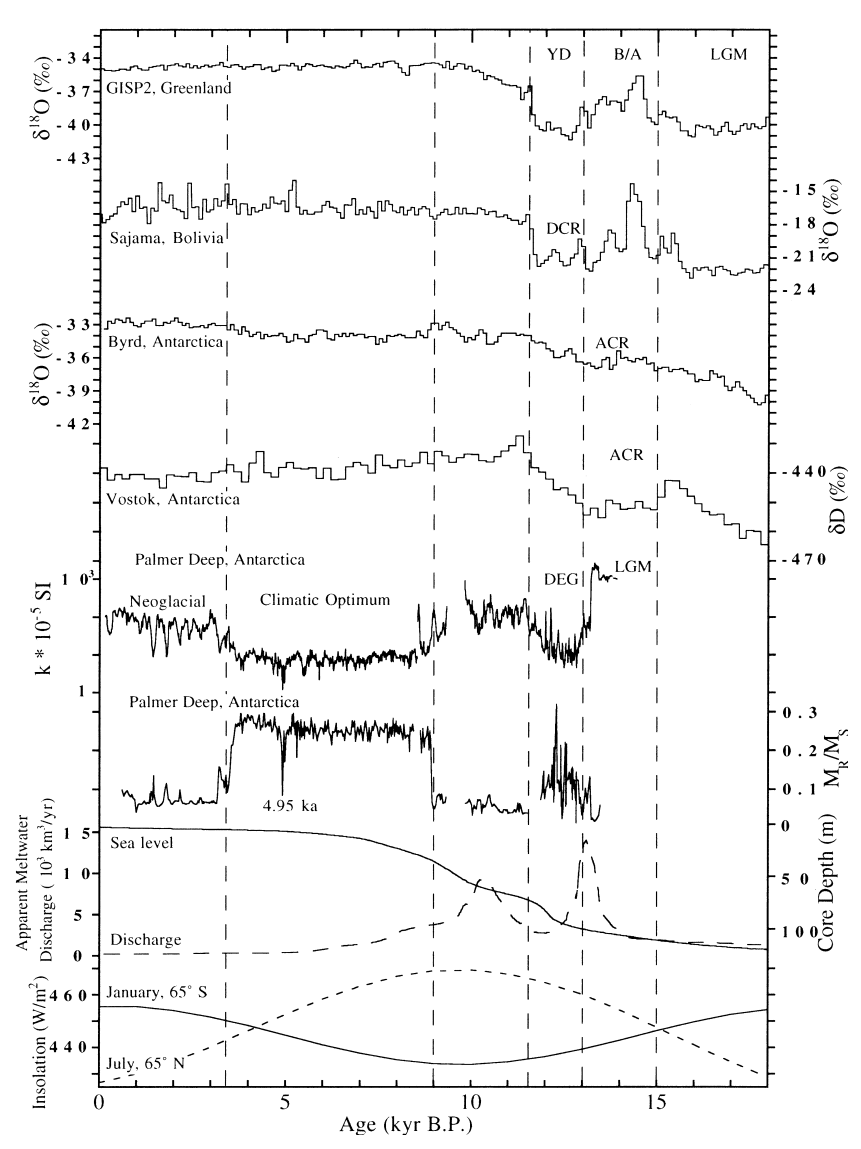


Fig. 6. Ice core  $\delta^{18}$ O records (100 year averages) from GISP2, Greenland [41], Sajama, Bolivia [40], Byrd, Antarctica [42],  $\delta D$  (200 year averages) from Vostok, Antarctica [43], k and  $M_R/M_S$  from the Palmer Deep, apparent meltwater discharge rate and sea level rise [46], and summer insolation curves for 65°N and 65°S [48]. LGM = Last Glacial Maximum, ACR = Antarctic Cooling Reversal, DCR = Deglaciation Cooling Reversal. The discharge curve from [46] is dated using calibrated <sup>14</sup>C ages. The true age of meltwater pulse 1a is likely ~1000 yr older than shown here based on U–Th calibration of the <sup>14</sup>C time scale [49]. However, the sea level curve from [46] is reservoir-corrected but not calibrated for variations in <sup>14</sup>C production rates. The retreat of grounded ice from the Palmer Deep (LGM) lags atmospheric warming in Antarctica by several thousand years. The Palmer Deep LGM/Deglaciation transition roughly coincides with meltwater pulse 1a. The Early Holocene interval in the Palmer Deep coincides with a minimum in southern hemisphere summer insolation and a maximum in the difference between summer heating of the two hemispheres. The Early Holocene interval also coincides with meltwater pulse 1b and a rapid rate of sea level rise. During this interval debris-laden icebergs may have been generated in response to increased calving due to sea level rise.

2500–4000 yr BP ([34,35] and references therein). The combination of marine ([3,4,6–17], this study) and land-based investigations (e.g. [36]) confirms the global occurrence of this climate shift. Similarly, the Palmer Deep record confirms the global nature of the Middle Holocene climatic optimum that is manifested as precipitation and humidity/aridity shifts in the tropics [37–40].

In contrast, the earliest portion of the Palmer Deep record is quite different from other polar and low latitude records [40-43] (Fig. 6). The synchronicity and interhemispheric phase relationships of ice core records are still a matter of debate [44,45]. Even with chronology uncertainties, it is clear that the post-LGM Palmer Deep records marine conditions that are not reflected in the ice cores. The LGM in the Palmer Deep lags atmospheric warming in the ice core records by several thousand years (Fig. 6). However, the LGM/Deglaciation transition in the Palmer Deep indicates when glacial ice retreated landward of the Palmer Deep and the basin became ice-free, which should lag atmospheric warming. Open water conditions and high productivity in the Palmer Deep occur soon after meltwater pulse 1a described in [46], supporting the idea of a lowdensity freshwater lid generated by a disintegrating ice sheet, leading to stabilization of the water column and high productivity.

The Early Holocene interval (11.5–9 ka) in the Palmer Deep is not seen in any of the ice core records. Although a cold event is documented at 8.2 ka [47], that feature is significantly younger and shorter than the Palmer Deep Early Holocene interval. The Early Holocene interval in the Palmer Deep does coincide with a minimum in southern hemisphere summer insolation and the time of the greatest difference in summer insolation received at the two poles [48]. This feature also coincides with meltwater pulse 1b described in [46] and with the most rapid rate of sea level rise following Deglaciation. Given that productivity in this interval is inferred to be higher than present levels [11], it is possible that the Early Holocene was not an interruption of post-glacial warming, but rather a function of the grounding line response to rising sea level.

# 6.7. Glacimarine sedimentation during the Holocene

Since magnetic susceptibility and granulometry reflect terrigenous sedimentation, the identification of sediment sources may yield additional information on depositional processes. This in turn may help identify the driving forces behind the Palmer Deep record. To try to understand the reasons for the five major shifts in magnetic material supplied to the Palmer Deep we examined the magnetic properties of possible source rock exposed along the western Antarctic Peninsula. Coarse-grained intrusives display MD hysteresis parameters and volcanic samples and sedimentary rocks display PSD hysteresis parameters [31]. The rocks display distinctive combinations of Verwey transition temperatures  $(T_{\rm V})$  and Curie temperatures  $(T_{\rm C})$ , which have the potential to be used as tracers of provenance in sediments. The magnetic properties of the Palmer Deep sediments and sediments from nearby fjords are more consistent

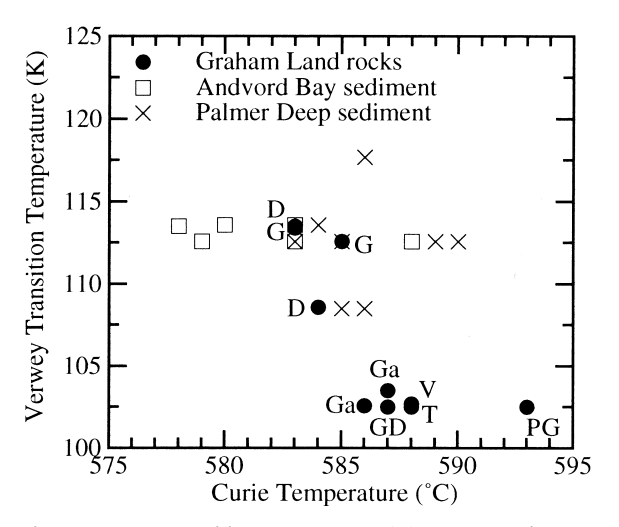


Fig. 7. Verwey transition temperature (K) versus Curie temperature (°C) for Palmer Deep sediments, Andvord Bay sediments, and rock samples from Northern Graham Land. G=granite, D=diorite, Ga=gabbro, GD=granodiorite, T=tonalite, PG=pink granite, V=volcanic. The calc-alkaline rocks of the Andean Intrusive Suite define two clusters. Sediments from the Palmer Deep and a nearby fjord, Andvord Bay, display magnetic properties that are consistent with a granite or diorite source rock. [31].

with a granite or diorite source rock (Fig. 7) and inconsistent with gabbros, granodiorites and tonalites. None of the Graham Land rock samples examined here contains TM40–TM60.

These observations make the Middle Holocene interval of the Palmer Deep record all the more intriguing. MD magnetite is abundant in the rocks near the Palmer Deep, and yet these grains were not deposited in the Palmer Deep during the Middle Holocene. Similarly, gravel grain counts are low during the Middle Holocene [6]. This suggests a reduction or cessation in iceberg generation, depriving the Palmer Deep of IRD.

Glaciers along the western Antarctic Peninsula are presently grounded below sea level [5]. The most extreme interpretation of the magnetic data suggests that glaciers terminated on land during the Middle Holocene. As sea level rose following Deglaciation, more of the glaciers would be exposed to waves and tides, causing an initial increase in calving and probably leading to retreat of termini. This process may explain the magnetic mineral assemblages in both the Early Holocene and Middle Holocene intervals. In this scenario, the Early Holocene interval represents the increased calving in response to rising sea level (Fig. 6), producing debris-laden icebergs. The Middle Holocene represents the retreat of the calving line and ultimate grounding of glaciers on land. Furthermore, diatom assemblages indicate a reduction in sea ice cover [12,13] during the Middle Holocene. A reduction in sea ice cover would mean less dampening of waves and therefore less protection of the glacial termini from ablation.

Alternatively, the absence of MD magnetite could simply indicate a shift in paleowind or paleocurrent patterns. At this time, drifting icebergs may not have passed over the Palmer Deep. The absence of MD magnetite could also be a function of iceberg survivability. Warmer water masses occupying the shelf during the Middle Holocene, as suggested by [7,13], may have accelerated the rate of melting of icebergs, resulting in the deposition of the coarse, dense grains closer to shore.

At present, we do not know the source of the titanium-rich titanomagnetite. Titanomagnetite with composition TM10-TM30 has been ob-

served in mafic dikes from this region, but not TM40-TM60 (S. Brachfeld, unpublished data). There may well be a local source that we have vet to examine. However, we suspect that TM60, a common component of oceanic crust, may be found further north near Bransfield Basin. If there were incursions of northerly sub-polar waters during the Middle Holocene, as suggested by diatom evidence [13], then TM60 may have been carried in suspension to the Palmer Deep. This mineral would dominate the magnetic mineral assemblage in the absence of locally derived MD magnetite. One other possibility worth discussion is eolian input. Titanomagnetite could be a wind-borne component of Andean volcanic dust originating in South American loess deposits. However, this is speculation at best. The closest ice core located on the Dyer Plateau [50] has extremely low dust concentrations. Furthermore, all micropaleontological evidence points to a stable water column, requiring less wind-driven mixing during the Middle Holocene. Locating the source of the titanium-rich titanomagnetite will be important for determining if the sediment assemblage during the Middle Holocene was derived from local or distal sources, which may indicate paleocurrent or paleowind directions along the western Antarctic Peninsula.

## 7. Conclusions

A 13 200-yr high-resolution sediment sequence from the Palmer Deep reveals a succession of five distinct paleoenvironmental intervals with superimposed century-scale cycles in productivity. The five paleoenvironmental intervals are defined by abrupt, large-amplitude changes in magnetic susceptibility and magnetic granulometry. Although variations in k are muted from 9 to 3.4 ka,  $\chi_{HF}$ demonstrates the persistence of century-scale cycles over the past 9000 yr. Each susceptibility zone contains a distinct magnetic mineral assemblage that reflects the variable supply of terrigenous material to the Palmer Deep. The LGM, the Early Holocene, and the Late Holocene are characterized by strong values of magnetic susceptibility and contain abundant coarse-grained MD magnetite. The correspondence of MD magnetite with the occurrence of gravel grains suggests that MD magnetite may serve as a proxy of sediment transport by icebergs. The Deglaciation and the Middle Holocene intervals contain finer grained magnetic particles, suggesting changes in sediment provenance and/or sediment transport. The finer grained assemblage of the Deglaciation interval was likely deposited by sub-glacial meltwater plumes. The Middle Holocene interval is characterized by the presence of PSD titanium-rich titanomagnetite and the complete absence of MD magnetite. The absence of MD magnetite, which is abundant in the surrounding rocks, suggests either a reduction in the local generation of icebergs, a decrease in iceberg survivability, or a shift in the iceberg drift paths. The Early Holocene-Middle Holocene transition in terrigenous sedimentation could represent increased calving in response to sea level rise, causing retreat of the ice front to a position on land. Identifying the source of the titanium-rich titanomagnetite will be critical in understanding the sedimentation processes and the environmental conditions during the Middle Holocene.

#### Acknowledgements

We thank the members of the ODP Leg 178 Scientific party for discussions during and after Leg 178. We are particularly grateful to our Antarctic colleagues E. Domack, R. Dunbar, S. Ishman, A. Leventer, P. Manley, A. Shevenell, C. Sjunneskog, and F. Taylor for discussions and for making their Palmer Deep data available. A. Evans, K. Hatfield, F. Kyte, and J. Schuffert carried out physical properties and interstitial water chemistry measurements during ODP Leg 178. E. Youcha and A. Eller spent countless hours preparing samples and making hysteresis measurements. We thank L. Thompson and E. Thompson for providing data sets, and acknowledge the generous web-based sharing of data by several ice core groups. J. Stoner, E. Thomas and two anonymous reviewers provided thoughtful, constructive comments that improved this manuscript. Constructive comments were also provided by E. Cowan, G. Seltzer, M. Jackson, and R. Powell. This work was supported by a JOI/USSAC ODP Graduate Fellowship (to S.A.B.). This is Byrd Polar Research Center contribution #1234 (IRM #0002). The IRM is supported by grants from the Earth Sciences Instrumentation and Facilities program of the National Science Foundation and the W.M. Keck Foundation. [RV]

#### References

- G.H. Denton, M.L. Prentice, L.H. Burckle, Cainozoic history of the Antarctic Ice Sheet, in: R.J. Tingey (Ed.), The Geology of Antarctica, Chapter 10, Clarendon Press, Oxford, 1991, pp. 365–433.
- [2] R. Smith, E.W. Domack, S. Emslie, W. Fraser, D. Ainley, K. Baker, J. Kennett, A. Leventer, E. Mosely-Thompson, S. Stammerjohn, M. Vernet, Marine ecosystem sensitivity to climate change, Bioscience 49 (1999) 393–404.
- [3] A. Leventer, E.W. Domack, S.E. Ishman, S. Brachfeld, C.E. McClennen, P. Manley, Productivity cycles of 200– 300 years in the Antarctic Peninsula region: understanding linkages between the Sun, atmosphere, sea ice and biota, Geol. Soc. Am. Bull. 108 (1996) 1626–1644.
- [4] F. Taylor, J. Whitehead, E. Domack, Holocene paleoclimate change in the Antarctic Peninsula: evidence from the diatom sedimentary and geochemical record, Mar. Micropaleontol. 41 (2000) 25–43.
- [5] T.W. Griffith, J.B. Anderson, Climatic control of sedimentation in bays and fjords of the Northern Antarctic Peninsula, Mar. Geol. 85 (1989) 181–204.
- [6] E.W. Domack, A. Leventer, R. Dunbar, F. Taylor, S. Brachfeld, and ODP Leg 178 Shipboard Scientific Party, Holocene Climate Variability in the Antarctic Peninsula, Holocene 11 (2001) 1–9.
- [7] A.E. Shevenell, J.P. Kennett, Antarctic Holocene climate change: stable isotopic record from the Palmer Deep, Paleoceanography, in press.
- [8] S.E. Ishman, M.R. Sperling, Benthic foraminiferal record of Holocene oceanographic evolution in the Palmer Deep, western Antarctic Peninsula, EOS Trans. AGU 82 (2001) S225.
- [9] R.B. Dunbar, A.C. Ravelo, E. Domack, A. Leventer, L. Anderson, D.A. Mucciarone, S. Brachfeld, 13,000 years of decadal-to-millennial oceanographic variability along the Antarctic Peninsula: ODP Site 1098, EOS Trans. AGU 81 (2000) F688.
- [10] L.D. Anderson, A.C. Ravelo, Data report: Biogenic opal in Palmer Deep sediments, Site1098 Leg 178, in: P.F. Barker, A. Camerlenghi, G.D. Acton, A.T.S. Ramsay (Eds.), Proc. ODP, Sci. Results, 178, available from World Wide Web: http://www-odp.tamu.edu/publications/178\_SR/chap\_01/chap\_01.htm.
- [11] C. Sjunneskog, F. Taylor, Postglacial marine diatom rec-

- ord of the Palmer Deep, Antarctic Peninsula (ODP Leg 178, Site 1098) I: Total diatom abundance, Paleoceanography, in press.
- [12] F. Taylor, C. Sjunneskog, Postglacial marine diatom record of the Palmer Deep, Antarctic Peninsula (ODP Leg 178, Site 1098) II: Diatom assemblages, Paleoceanography, in press.
- [13] A. Barkoukis, A. Leventer, Laminations from the Palmer Deep, Antarctica, Antarct. J. U.S., in press.
- [14] A. Leventer, E. Domack, A. Barkoukis, B. McAndrews, J. Murray, Laminations from the Palmer Deep: a diatombased interpretation, Paleoceanography, in press.
- [15] J. Pike, S.G. Moreton, C.S. Allen, Data report: Microfabric analysis of deglacial sediments from the Palmer Deep, western Antarctic Peninsula, in: P.F. Barker, A. Camerlenghi, G.D. Acton, A.T.S. Ramsay (Eds.), Proc. ODP, Sci. Results, 178, Ocean Drilling Program, College Station, TX, in press.
- [16] K. Kryc, R. Murray, Millennial-scale changes in export production and terrigenous character documenting Holocene climate instability in sediments from the Palmer Deep, west Antarctic Peninsula, EOS Trans. AGU 81 (2000) F688.
- [17] N.R. Warner, E.W. Domack, Millennial to decadal scale paleoenvironmental change during the Holocene in the Palmer Deep, Antarctica as recorded by particle size analysis, Paleoceanography, in press.
- [18] M. Rebessco, A. Camerlenghi, L. DeSantis, E.W. Domack, M.E. Kirby, Seismic stratigraphy of Palmer Deep: a fault bounded late Quaternary sediment trap on the inner continental shelf, Antarctic Peninsula Pacific margin, Mar. Geol. 151 (1998) 89–110.
- [19] P.F. Barker, A. Camerlenghi, G.D. Acton, and the ODP Leg 178 Scientific Party, Proc. Ocean Drilling Program, Initial Reports 178, 1998.
- [20] G.D. Acton, C.J. Borton, and the Leg 178 Shipboard Scientific Party, Palmer Deep composite depth scales for Leg 178 Sites 1098 and 1099, in: P.F. Barker, A. Camerlenghi, G.D. Acton, A.T.S. Ramsay (Eds.), Proc. ODP, Sci. Results, 178, available from World Wide Web: http:// www-odp.tamu.edu/publications/178\_SR/chap\_05/chap\_05.htm.
- [21] S.A. Brachfeld, S.K. Banerjee, Rock-magnetic carriers of century-scale susceptibility cycles in glacial-marine sediments from the Palmer Deep, Antarctic Peninsula, Earth Planet. Sci. Lett. 176 (2000) 443–455.
- [22] D.E. Canfield, R.A. Berner, Dissolution and pyritization of magnetite in anoxic marine sediments, Geochim. Cosmochim. Acta 51 (1987) 645–659.
- [23] R. Day, M.D. Fuller, V.A. Schmidt, Hysteresis properties of titanomagnetites: Grain size and composition dependence, Phys. Earth Planet. Int. 13 (1977) 260–266.
- [24] D.J. Dunlop, O. Ozdemir, Rock Magnetism: Fundamentals and Frontiers, Cambridge University Press, 1997.
- [25] B.M. Moskowitz, R.G. Frankel, D.A. Bazylinski, Rock magnetic criteria for the detection of biogenic magnetite, Earth Planet. Sci. Lett. 120 (1993) 283–300.

- [26] B.M. Moskowitz, M. Jackson, C. Kissel, Low-temperature magnetic behavior of titanomagnetites, Earth Planet. Sci. Lett. 157 (1998) 141–149.
- [27] Ö. Özdemir, D.J. Dunlop, B.M. Moskowitz, The effect of oxidation on the Verwey transition in magnetite, Geophys. Res. Lett. 20 (1993) 1671–1674.
- [28] P.W. Readman, W. O'Reilly, Magnetic properties of oxidized (cation-deficient) titanomagnetites, (Fe, Ti, [])O<sub>4</sub>, J. Geomagn. Geoelectr. 24 (1972) 69–90.
- [29] C.P. Hunt, B.M. Moskowitz, S.K. Banerjee, Magnetic properties of rocks and minerals, in: T.J. Ahrens (Ed.), Rock Physics and Phase Relations: A Handbook of Physical Constants, vol. 3, Am. Geophys. Union, 1995, pp. 189–204.
- [30] M.J. Jackson, B.M. Moskowitz, J. Rosenbaum, C. Kissel, Field-dependence of AC susceptibility in titanomagnetites, Earth Planet. Sci. Lett. 157 (1998) 129–139.
- [31] S. Brachfeld, A. Grunow, E. Youcha, Magnetic properties of igneous and meta-sedimentary rocks from Graham Land, Antarctic Peninsula, Antarct. J. U.S., in press.
- [32] J. Jouzel, N.I. Barkov, L.H. Burckle, Y. Duclos, V.M. Kotlyakov, C. Lorius, M. Martin, M.A. Melieres, J.R. Petit, M. Stievenard, M. Toots, R. Vaikmae, The two-step shape and timing of the last deglaciation in Antarctica, Clim. Dyn. 11 (1995) 151–161.
- [33] C.J. Pudsey, P.F. Barker, R.D. Larter, Ice sheet retreat from the Antarctic Peninsula shelf, Cont. Shelf Res. 14 (1994) 1647–1675.
- [34] G.H. Denton, W. Karlén, Holocene climatic variations their patterns and possible causes, Quat. Res. 3 (1973) 155–205.
- [35] S. Porter, Onset of Neoglaciation in the Southern Hemisphere, J. Quat. Sci. 15 (2000) 395–408.
- [36] Ó Ingólfsson, C. Hjort, P.A. Berkman, S. Björck, E. Colhoun, I.D. Goodwin, B. Hall, K. Hirakawa, M. Melles, P. Möller, M.L. Prentice, Antarctic glacial history since the last glacial maximum: an overview of the record on land, Antarct. Sci. 10 (1998) 326–344.
- [37] P.A. Baker, G.O. Seltzer, S.C. Fritz, R.B. Dunbar, M.J. Grove, P.M. Tapia, S.L. Cross, H.D. Rowe, J.P. Broda, The history of South American tropical precipitation for the past 25,000 years, Science 291 (2001) 640–643.
- [38] G.H. Haug, K.A. Hughen, D.M. Sigman, L.C. Peterson, U. Röhl, Southward migration of the intertropical convergence zone through the Holocene, Science 293 (2001) 1304–1308.
- [39] P. de Menocal, J. Ortiz, T. Guilderson, M. Sarnthein, Coherent high- and low-latitude variability during the Holocene warm period, Science 288 (2000) 2198– 2202.
- [40] L.G. Thompson, M.E. Davis, E. Mosley-Thompson, T.A. Sowers, K.A. Henderson, V.S. Zagorodnov, P.-N. Lin, V.N. Mikhalenko, R.K. Campen, J.F. Bolzan, J. Cole-Dai, B. Francou, A 25,000-year tropical climate history from Bolivian ice cores, Science 282 (1998) 1858–1864.
- [41] P.M. Grootes, M. Stuiver, J.W.C. White, S. Johnsen, J. Jouzel, Comparison of oxygen isotope records from the

- GISP2 and GRIP Greenland ice cores, Nature 366 (1993) 552–554.
- [42] S.J. Johnsen, W. Dansgaard, H.B. Clausen, C.C. Langway Jr., Oxygen isotope profiles through the Antarctic and Greenland ice sheets, Nature 235 (1972) 429–434.
- [43] J. Jouzel, C. Lorius, J.R. Petit, C. Genthon, N.I. Barkov, V.M. Kotlyakov, V.M. Petrov, Vostok ice core: An continuous isotope temperature record over the last climatic cycle (160,000 years), Nature 329 (1987) 403– 408
- [44] T. Blunier, J. Chappellaz, J. Schwander, A. Dällenbach, B. Stauffer, F.F. Stocker, D. Raynaud, J. Jouzel, H.B. Clausen, C.U. Hammer, S.J. Johnsen, Asynchrony of Antarctic and Greenland climate change during the last glacial period, Science 394 (1998) 739–743.
- [45] E.J. Steig, D.L. Morse, E.D. Waddington, M. Stuiver, P.M. Grootes, P.A. Mayewski, M.S. Twickler, S.I. Whitlow, Wisconsin and Holocene climate history from an ice core at Taylor Dome, western Ross Embayment, Antarctica, Geogr. Ann. 82A (2000) 213–235.

- [46] R.G. Fairbanks, A 17,000-year glacio-eustatic sea level record: Influence of glacial melting on the Younger Dryas Event and deep ocean circulation, Nature 342 (1989) 637– 642
- [47] R.B. Alley, P.A. Mayewski, T. Sowers, M. Stuiver, K.C. Taylor, P.U. Clark, Holocene climate instability: a prominent widespread event 8200 y ago, Geology 25 (1997) 483–486.
- [48] A. Berger, M.F. Loutre, Insolation values for the climate of the last 10 million years, Quat. Sci. Rev. 10 (1991) 297– 317.
- [49] E. Bard, B. Hamelin, R.G. Faribanks, A. Zindler, Calibration of the <sup>14</sup>C timescale over the past 30,000 years using mass spectrometric U–Th ages from Barbados corals, Nature 345 (1990) 405–410.
- [50] L.G. Thompson, D.A. Peel, E. Mosley-Thompson, R. Mulvaney, J. Dai, P.N. Lin, M.E. Davis, C.F. Raymond, Climate since AD 1510 on Dyer Plateau, Antarctic Peninsula: evidence for recent climate change, Ann. Glaciol. 20 (1994) 420–426.